Electrochemical and FTIR Spectroscopic Characterization of the Cytochrome bc_1 Complex from *Paracoccus denitrificans*: Evidence for Protonation Reactions Coupled to Quinone Binding†

Michaela Ritter,‡ Oliver Anderka,§ Bernd Ludwig,§ Werner Mäntele,‡ and Petra Hellwig*,‡

Institut für Biophysik, Johann Wolfgang Goethe-Universität, Theodor-Stern-Kai 7, Haus 74, 60590 Frankfurt am Main, Germany, and Institut für Biochemie, Abteilung Molekulare Genetik, Johann Wolfgang Goethe-Universität, Marie-Curie-Strasse 9, 60439 Frankfurt am Main, Germany

Received June 26, 2003; Revised Manuscript Received August 25, 2003

ABSTRACT: The cytochrome bc_1 complex from *Paracoccus denitrificans* and soluble fragments of its cytochrome c_1 and Rieske ISP subunits are characterized by a combined approach of protein electrochemistry and FTIR difference spectroscopy. The FTIR difference spectra provide information about alterations in the protein upon redox reactions: signals from the polypeptide backbone, from the cofactors, and from amino acid side chains. We describe typical modes for conformational changes in the polypeptide and contributions of different secondary structure elements. Signals attributed to the different cofactors can be presented on the basis of selected potential steps. Modes associated with bound quinone are identified by comparison with spectra of quinone in solution at 1656, 1642, and 1610 cm^{-1} and between 1494 and 1388 cm^{-1}, as well as at 1288 and 1262 cm^{-1}. Signals originating from the quinone bound at the Q_o site can be distinguished. On the basis of the infrared data, the total quinone concentration is determined to be 2.6−3.3 quinones per monomer, depending on preparation conditions. The balance of evidence supports the double-occupancy model. Interestingly, the amplitude of the band at 1746 cm^{-1} increases with quinone content, reflecting a protonation reaction of acidic groups. In this context, the involvement of glutamates and/or aspartates in the vicinity of the Q_o site is discussed on the basis of recently determined crystal structures.

Ubiquinol-cytochrome *c* oxidoreductase [cytochrome bc_1 complex, complex III (*1*)] is one of the fundamental components of the respiratory electron transfer chains located in the inner mitochondrial or bacterial cytoplasmic membrane. The enzyme couples the electron transfer from ubiquinol to cytochrome *c* to translocation of protons across the membrane. As a minimum requirement, all bc_1 complexes contain three catalytic subunits: cytochrome *b* with two *b*-type hemes (cytochrome b_L and b_H), cytochrome c_1 with a covalently bound *c*-type heme, and the Rieske iron−sulfur protein with a [2Fe-2S] cluster (ISP).[1] Crystal structures of the mitochondrial complexes, which contain additional subunits, have been reported (*2*−*5*). The cytochrome bc_1 complex of *Paracoccus denitrificans* represents a small bacterial version of this enzyme lacking any additional subunits. Its X-ray structure is as yet unknown; however, a similar architecture for the three catalytic subunits can be inferred.

Both bacterial and mitochondrial bc_1 complexes follow the same catalytic mechanism, the so-called Q cycle (*6*−*8*), which relies on two separate binding sites for quinones, Q_o and Q_i. The Q_o site is located close to heme b_L and the [2Fe-2S] cluster, whereas the Q_i site is near heme b_H on the other side of the membrane. The Q cycle comprises two identical half-reactions, leading to the oxidation of two quinol molecules at the Q_o site. With each quinol oxidation step, two electrons that undergo a bifurcation reaction are released. One electron is transferred via the ISP and cytochrome c_1 to reduce cytochrome *c*. The other is transferred to the Q_i site via heme b_L and heme b_H. In the first quinol oxidation step, this electron is used to reduce quinone to semiquinone at Q_i, followed by further reduction to quinol after the oxidation of the second quinol at Q_o. In the quinone reduction reaction at Q_i, two protons are taken up from the negative side of the membrane, whereas quinol oxidation releases four protons on the positive side, resulting in an electrochemical proton gradient for ATP production. Although this mechanism is generally accepted, not all aspects of the quinol/quinone binding and reaction are yet fully understood at the molecular level. Especially, for the quinol oxidation mechanism at the Q_o site different models are discussed (*9*−*13*).

† This work is supported by Deutsche Forschungsgemeinschaft (SFB 472).

* To whom correspondence should be addressed. E-mail: hellwig@biophysik.uni-frankfurt.de. Phone: +49-69-6301-4227. Fax: +49-69-6301-5838.

‡ Institut für Biophysik, Johann Wolfgang Goethe-Universität.

§ Institut für Biochemie, Abteilung Molekulare Genetik, Johann Wolfgang Goethe-Universität.

[1] Abbreviations: IR, infrared; FTIR, Fourier transform infrared; UV−vis, ultraviolet−visible; ISP, Rieske iron−sulfur protein; ISF, soluble Rieske iron−sulfur protein fragment; cyt, cytochrome; bc_1 complex, ubihydroquinone:cytochrome *c* oxidoreductase; b_H, high-potential *b*-type heme; b_L, low-potential *b*-type heme; Q_o, ubiquinol oxidation site; Q_i, ubiquinone reduction site; SHE′, standard hydrogen electrode (for pH 7); DDM, *n*-dodecyl β-D-maltoside; THF, tetrahydrofuran.

10.1021/bi035103j CCC: $25.00
Published on Web 09/26/2003

FTIR difference spectroscopy is a sensitive method for detecting even subtle structural changes occurring during the redox reactions of the enzyme. In this study, we investigate the bc_1 complex from *P. denitrificans* by a combination of protein electrochemistry and FTIR difference spectroscopy, a method established for several membrane proteins as described previously (*14*−*16*). We present the FTIR difference spectra of the complex, and tentatively assign redox-dependent signals in this spectra from (a) cofactors, (b) changes in the protein backbone, and (c) contributions of individual amino acid side chains involved in the electron transfer reaction. Selected potential steps allow the assignment of vibrational modes to the different cofactors. Additional attributions are made by analyzing the spectra of the water-soluble fragments of cytochrome c_1 and Rieske ISP, as well as the quinone in solution. We describe FTIR difference spectra that differ in the quinone content and give an estimation of the number of quinones bound to the complex and distinguish modes of the quinone bound to Q_o.

MATERIALS AND METHODS

Sample Preparation. The *fbc* operon encoding the *P. denitrificans* bc_1 complex was cloned into the *Hin*dIII and *Sac*I sites of the pRI2 vector (*17*). The plasmid was conjugated into an *fbc* deletion mutant of *P. denitrificans* (*18*), resulting in a strain overexpressing the enzyme. Cell growth, membrane isolation and solubilization, subsequent protein purification, and determination of enzyme activity were performed essentially as described in ref *19*, with the following modifications. (1) Solubilized membranes were diluted to a salt (NaCl) concentration of 350 mM with 50 mM MES/NaOH (pH 6.0) and 0.02% (w/v) *n*-dodecyl β-D-maltoside (DDM) before anion exchange chromatography. (2) A salt gradient between 350 and 600 mM NaCl was applied. For elution, pooled fractions were concentrated by ultrafiltration (Amicon Centriprep/Centricon, exclusion limit of 100 kDa), equilibrated with the standard buffer for the FTIR experiments [100 mM phosphate buffer (pH 7), 150 mM KCl, and 0.02% DDM] by gel filtration (Sephadex G25 fine), and afterward ultrafiltered again to a final concentration of approximately 0.5 mM.

Exchange of H_2O against D_2O was performed by concentrating the enzyme several times and rediluting it in the corresponding D_2O buffer (pD 7). H−D exchange was found to be more than 80% complete, as judged from the shift of the amide II mode at 1550 cm^{-1} (data not shown). For measurements at different pH conditions, buffer exchange was performed analogously. The following buffer solutions were used: 200 mM cacodylate buffer for pH 5.5, 100 mM phosphate buffer for pH 6, and 200 mM borate buffer for pH 8, with all buffers containing 100 mM KCl and 0.02% DDM.

The purification of the soluble Rieske fragment (ISF) was adapted from previously described protocols (*21*, *22*). The purified bc_1 complex was obtained in 20 mM Tris-HCl (pH 8), 100 mM NaCl, and 0.02% DDM. The protein concentration was adjusted to 10 mg/mL, and 5 mM $CaCl_2$ and 0.2% sodium deoxycholate were added. Limited proteolysis of the complex was performed with thermolysin [Sigma; 1:100 (w/w) protease:bc_1 ratio] for 2 h at room temperature, and stopped by addition of 5 mM EDTA. A major portion of cytochromes *b* and c_1 could be removed as they stuck on a hydroxyapatite column, while ISF could be eluted after washing with 10 mM potassium phosphate (pH 7.2) and 150 mM KCl. Following dialysis against a buffer containing 50 mM potassium phosphate (pH 8) and 10 mM KCl, the ISF fraction was applied to a Mono Q HR 5/5 column (Pharmacia). After the mixture had been washed with 50 mM potassium phosphate (pH 8), 10 mM KCl, and 0.1% DDM, the ISF was eluted at 200 mM KCl with a linear salt gradient [from 0 to 300 mM KCl with 50 mM potassium phosphate (pH 8)]. The sample was concentrated by ultrafiltration (Vivaspin 3 kDa, Vivascience), applied to a Superdex 200 gel filtration column (Pharmacia), and eluted with 100 mM potassium phosphate (pH 7) and 150 mM KCl. The final preparation was concentrated to ∼0.5 mM and stored at −80 °C. SDS−PAGE, Western blotting, and UV−vis and EPR spectroscopy confirmed the purity and identity of the ISF (data not shown). The isolated cytochrome c_1 fragment was purified as described previously (*23*). For spectroelectrochemistry, the isolated subunit fragments were taken up in 100 mM phosphate buffer (pH 7), containing a minimum of 100 mM KCl as a supporting electrolyte.

Electrochemistry. The ultra-thin layer spectroelectrochemical cell was used as described previously (*15*, *24*, *25*). To avoid irreversible protein adhesion, the gold grid working electrode was modified with a 2 mM cysteamine solution for 1 h and then washed with deionized water. To accelerate the redox reactions, a mixture of 17 mediators (see ref *16*, except for diethyl 3-methylparaphenylenediamine and dimethylparaphenylenediamine, but adding quinhydrone) was added in a substoichiometric concentration of 40 μM to the protein solution. The solution (7−8 μL) was used to fill the electrochemical cell. The cell path length was less than 10 μm, as determined at the beginning of each experiment. All experiments were performed at 278 K. Potentials are given with respect to the standard hydrogen electrode (SHE′) at pH 7.

Spectroscopy. FTIR and UV−vis difference spectra were simultaneously recorded as a function of the applied potential using a setup combining an IR beam from the interferometer (modified IFS 25, Bruker) for the 4000−1000 cm^{-1} range and a dispersive spectrometer for the 400−900 nm range as reported previously (*24*, *26*). First, the protein was equilibrated at an initial electrode potential, and a single-beam spectrum was recorded. Then the final potential was applied, and a single-beam spectrum was again recorded after equilibration. Equilibration generally took less than 4 min for the full potential step from −0.292 to 0.708 V. To resolve the spectra of individual cofactors with selected potential steps, significant higher equilibration times were required. Difference spectra as presented here were calculated from two single-beam spectra, with the initial spectrum taken as a reference. Typically, 128 interferograms at 4 cm^{-1} resolution were coadded for each single-beam spectrum, and Fourier transformed using triangular apodization and a zero filling factor of 2. Eight to ten difference spectra were averaged. To take into account differences in sample concentration and path length, the FTIR difference spectra were normalized on the difference signals of the α-band in the UV−vis spectrum (not shown).

Quinone Content. The quinone content in the sample was determined using the absorption band of the methoxy side

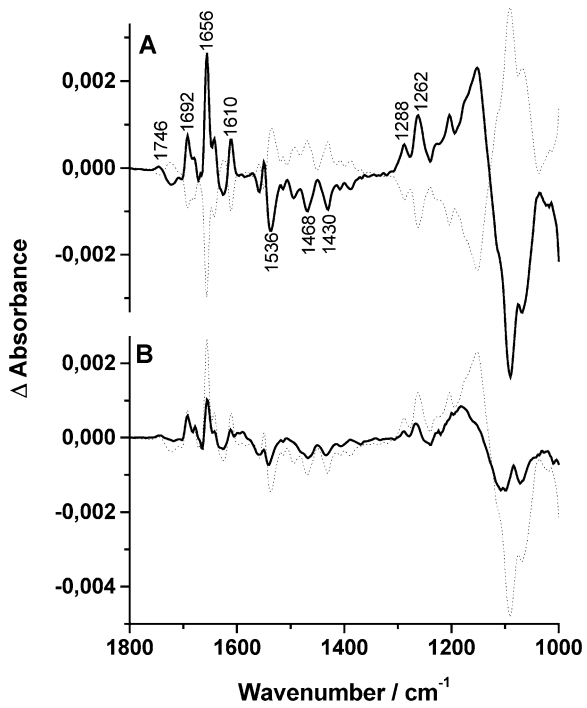

FIGURE 1: Electrochemically induced FTIR difference spectra of the cytochrome bc_1 complex from *P. denitrificans* obtained for a potential step from −0.292 to 0.708 V. (A) Oxidized-minus-reduced spectrum (thick line) and reduced-minus-oxidized spectrum (dotted line) of a sample equilibrated in phosphate buffer (pH 7). (B) Oxidized-minus-reduced spectrum of the sample equilibrated in the corresponding D_2O buffer (thick line). The dotted line shows the H_2O spectrum. The spectra are normalized to the same concentration according to the α-band (553/559 nm) in the visible spectral range.

chain of the quinone typically observed at 1262 cm^{-1}. Therefore, we measured the amount of free UQ_{10} in a tetrahydrofuran solution (THF) at distinct concentrations of 3−50 mM in an infrared cell consisting of two CaF_2 windows with a defined path length. On the basis of the calculated extinction coefficient ϵ at 1262 cm^{-1}, corresponding to a value of 0.4 mM^{-1} cm^{-1}, the unknown quinone concentration of the protein sample was determined for different preparations. The vibrational mode involving coordinates of the C−OCH_3 side chain was observed to be especially insensitive to the direct environment, in different solvents as in different proteins. The evaluation of the spectra in water and THF resulted in the same extinction coefficient.

RESULTS

Electrochemically Induced FTIR Difference Spectra of the P. denitrificans bc_1 Complex. Figure 1A shows the oxidized-minus-reduced (thick line) and reduced-minus-oxidized (dotted line) difference spectra of the bc_1 complex from *P. denitrificans* obtained for a potential step from −0.292 to 0.708 V in the spectral range of 1800−1000 cm^{-1}. Figure 1B shows the oxidized-minus-reduced spectrum recorded after equilibration in D_2O buffer (thick line), in direct comparison to the spectrum of the sample in H_2O buffer (dotted line). The spectra are normalized using the peaks at 553 and 559 nm in the UV−vis difference spectrum (not shown). In the oxidized-minus-reduced FTIR difference spectra, positive bands represent signals associated with the oxidized state of the protein and negative bands signals with the reduced state. The spectra in Figure 1A are mirror images, indicating a fully reversible redox reaction at the working electrode. This reversibility is also observed for the D_2O spectra (data not shown). Generally, in the given spectral range, signals from conformational changes of the protein backbone and the cofactors will appear, as well as protonation and deprotonation reactions of the amino acid side chains. Three main regions can be distinguished: the 1690−1620 cm^{-1} region (amide I), the 1560−1520 cm^{-1} region (amide II), and the region from 1100 to 1000 cm^{-1}, where contributions of the phosphate buffer dominate the spectrum.

The amide I modes predominantly result from C═O stretch vibrations of the polypeptide backbone. Characteristic absorptions for the different secondary structure elements can be distinguished (*45*). The electrochemically induced FTIR spectrum in Figure 1A shows strong positive bands in the amide I region; the band at 1650 cm^{-1} includes signals from the predominantly α-helical structure of the enzyme.

The coupled CN stretching and NH bending modes of the backbone contribute in the amide II region. The H−D exchange experiment of Figure 1B can be used to assess the contribution of the amide II signals to the observed redox difference spectra. If bands in the region from 1560 to 1520 cm^{-1} were principally due to amide II vibrations, the deuterium exchange would uncouple CN stretching and NH bending modes and shift the peak to ∼1480 cm^{-1}. Since no clear shifts can be seen in Figure 1B, contributions of the amide II modes can be excluded.

The difference spectra are strongly dominated by quinone signals. Some of the quinone is lost after buffer exchange. This includes the H−D exchange experiment and explains several shifts in the amide I range and, for example, at 1262 cm^{-1}. On the basis of direct comparison with isolated quinone (*36*) and samples with different quinone contents, contributions from the bound quinone are found from 1700 to 1200 cm^{-1} and will be described in a following paragraph.

Modes from the three hemes (b_L, b_H, and c_1), including signals from the heme propionates, vinyl side chains, and the porphyrin ring itself, are expected, and will be discussed later in detail.

Signals from the Rieske [2Fe-2S] cluster itself cannot be found in the investigated spectral range, because the Fe−S vibration mode is present at lower frequencies. However, alterations of the backbone and amino acid side chains of the direct cluster environment may contribute to the spectrum.

Overall, the spectrum shown here contains a significant number of overlapping bands. A summary of tentative assignments for the overall bc_1 spectrum based on a detailed analysis of the signals given in the following paragraphs is listed in Table 1.

Discrimination of Individual Contributions in the Overall Spectrum. For analyzing the contributions of the individual cofactors and their vicinities with regard to the overall spectrum, we followed two different strategies: (1) spectral separation of the cofactors on the basis of their midpoint potentials in the intact enzyme and (2) investigation of isolated water-soluble fragments of the bc_1 complex. The midpoint potentials of the *b*-type hemes determined in this work using potentiometric titrations in the visible spectral range are comparable with published data (*27*). The heme c_1 potential published as +180 mV (*44*) differs significantly from our results, which range from 268 to 338 mV. The

Table 1: Tentative Assignments for the Electrochemically Induced FTIR Spectrum of the *P. denitrificans* bc_1 Complex Shown in Figure 1A[a]

band position (cm^{-1})	assignment
1746(+)	ν(C═O) Asp/Glu
1710(+)	ν(C═O) Asp/Glu (cyt b_H)
1692(+)	amide I (Rieske β-sheet)
	ν(C═O) heme propionates b_L, b_H
1680(+)	ν(C═O) heme propionates b_L, b_H, c_1
	ν(C═O) Gln/Asn (cyt b_H)
	amide I (Rieske loop structures)
1670(+)	$\nu(CN_3H_5)$ Arg (cyt b_H)
1656(+)	amide I (α-helical, unordered)
	ν(C═O) quinone
1642(+)	ν(C═O) quinone
	ν_{37} heme c_1
1630(+,s)	amide I (Rieske β-sheet)
	$\nu(CN_3H_5)$ Arg (cyt b_H)
1610(+)	ν(C═C) quinone
1592(+)	
1570(+)	amide II
	ν_{37} heme b_L
	ν_{38} heme c_1
1558(−)	$\nu(COO^{-as})$ heme propionates b_L, b_H, c_1
	$\nu(COO^{-as})$ Asp/Glu (cyt b_H)
1550(+)	amide II
	ν_{38} heme b_H
1536(−)	amide II
	$\nu(COO^{-as})$ Asp/Glu (cyt b_H)
	$\nu(COO^{-as})$ heme propionates b_L, b_H
1518(+)	amide II
1506(+)	amide II (Rieske)
1494(−)	quinone ring
1468(−)	quinone ring
1430(−)	quinone ring
1408(−)	quinone ring
1388(−)	quinone ring
	$\nu(COO^{-s})$ Asp/Glu (cyt b_H)
1368(−)	$\nu(COO^{-s})$ heme propionates
	$\nu(COO^{-s})$ Asp/Glu (cyt b_H)
1288(+)	ν(C−O) methoxy group, quinone
1262(+)	ν(C−O) methoxy group, quinone
	ν_{42} heme c_1
1240(−)	ν_{42} heme b_H
	ν_{42} heme c_1
1204(+)	quinone
1176(+)	
1152(+)	
1090	P═O buffer
1068	P═O buffer

[a] Positive signals describing the oxidized state of the complex (+), the reduced state (−), and the shoulder (s). For details, see the text.

Table 2: Midpoint Potentials of the bc_1 Cofactors from *P. denitrificans* (pH 7) Determined in Potentiometric Titrations for the Spectral Range from 400 to 700 nm

cofactor	midpoint potential (mV)
heme b_L	−92
heme b_H	+58
heme c_1	268−338
heme c_1 (isolated cyt c_1 fragment)	+163
Rieske ISP	313[a]

[a] From ref *19*.

reason for this variation is not known, but in previous publications, a wide range for the c_1 potential in mitochondria was also found (*46*). For the isolated cytochrome c_1 fragment, we found a midpoint potential of 163 mV, significantly lower than that of the bound form. Since the separation of the subunit may induce a shift of the midpoint potential, we attribute the shift to the loss of the interaction with the overall complex. For investigation of the Rieske protein, we used an E_m value of 313 mV (*19*). All the values that were determined are listed in Table 2. Contributions of hemes b_L, b_H, and c_1 could be clearly separated by choosing a potential step according to their midpoint potential. The correct discrimination of the cytochrome contributions was controlled by simultaneously recording spectra in the visible region (shown in Figure 2A).

Contributions of Heme b_L. Figure 2B shows the oxidized-minus-reduced spectrum for a potential step from −0.292 to −0.022 V, where the redox reaction of heme b_L is expected. The spectrum includes only small absorption changes in comparison to the spectrum of the entire complex (dotted line). Very small but reproducible and reversible positive signals can be seen over the complete spectral range. The signal pattern of the amide I region is very similar to that of heme b_L from *Rhodobacter capsulatus* as observed at pH 6.5 (*14*). The band positions differ for approximately four wavenumbers in both spectra. Stronger signals can be found in the range of the amide I vibration at 1656, 1646, and 1636 cm^{-1}. These signals represent the C═O stretching modes of the polypeptide backbone. On the basis of heme model studies, likely candidates for C═O modes of protonated heme propionates are the positive signals at 1690 and 1676 cm^{-1} (*28*). The modes characteristic of deprotonated heme propionates in cytochrome *c* oxidase have been determined by specific ^{13}C labeling at the propionates (*29*). On this basis, the signals are expected in the range from 1570 to 1530 cm^{-1} for the antisymmetric COO^- vibration. The negative signals at 1560 and 1540 cm^{-1} are tentatively assigned to this vibration, whereas a possible candidate for the symmetric COO^- vibration can be found at 1372 cm^{-1}. The C═C vibrations of the vinyl substituent are expected to be around 1620 cm^{-1}, where a signal is present in the spectrum shown in Figure 2B. In the case of the porphyrin ring, several vibrations are described (*30*). The *CaCm* vibration (ν_{37}) is expected in the range from 1655 to 1586 cm^{-1}, and several peaks are present in this region, with signals at 1602 and 1584 cm^{-1} being candidates for this vibration. In heme *b* model studies, the *CbCb* vibration (ν_{38}) was identified between 1604 and 1542 cm^{-1}, where a number of signals can be detected in our spectrum (*28*). A negative signal can be found at 1580 cm^{-1} and positive signals at 1570 and 1554 cm^{-1}. Conclusive assignments are difficult here, because of the possible involvement of COO^- vibrations.

Contributions of Heme b_H. Figure 2C shows the oxidized-minus-reduced spectrum for a potential step from −0.022 to 0.208 V, which is assigned to heme b_H. It is substantially similar to the spectrum of the whole complex (dotted line), but lacks typical quinone signals, which are also expected in this potential range. The heme reaction itself was complete, as observed in the spectrum in the visible spectral range shown in Figure 2A. Generally, the quinone reacts very slowly under conditions near its midpoint potential. After longer equilibration times (∼30−40 min), the quinone signals appear; however, the quality of the IR spectra is too poor for detector stability. This phenomenon was also observed for quinol oxidase (P. Hellwig, unpublished observations). To visualize the quinone signals, we measured and calculated a difference spectrum using selected potential steps (Figure

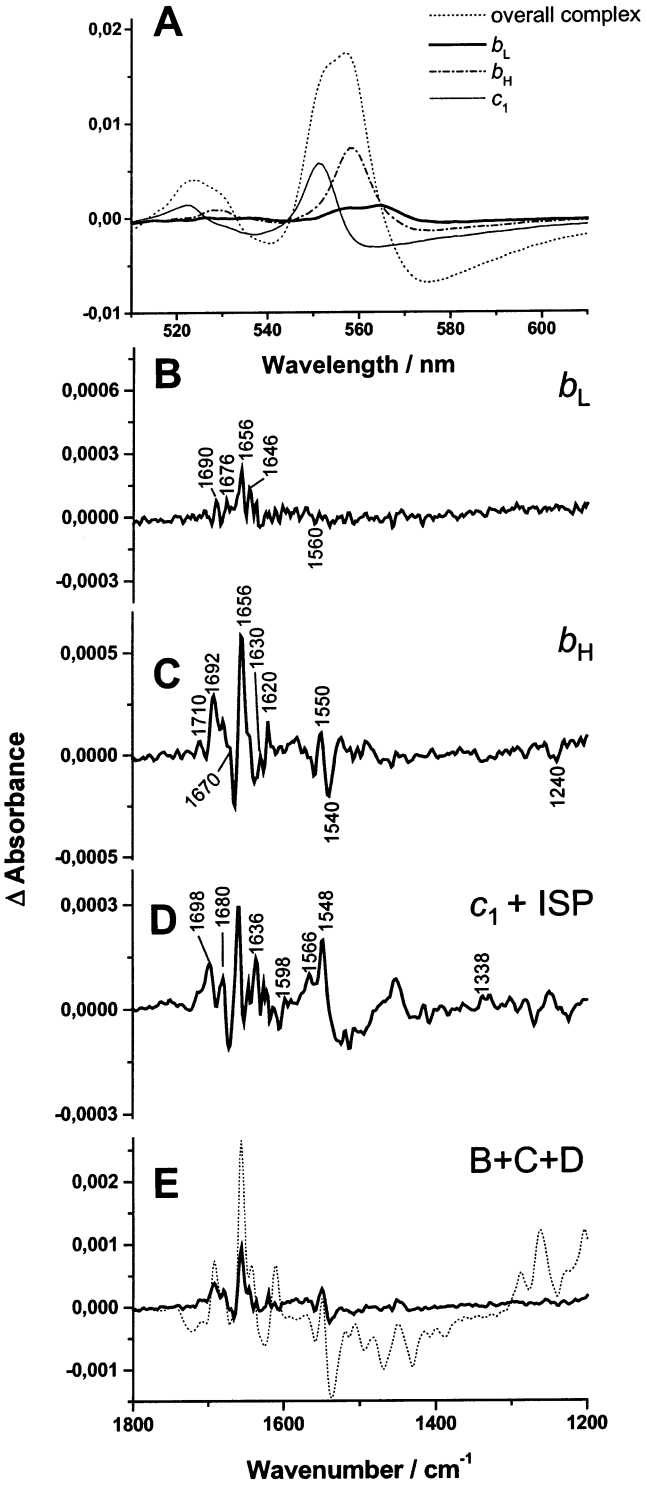

FIGURE 2: Oxidized-minus-reduced difference spectra of the bc_1 complex from *P. denitrificans* for selected potential steps. (A) Spectra in the region of the α- and *β*-band from 510 to 610 nm: b_L (thick solid line), b_H (dashed and dotted line), c_1 (thin solid line), and whole complex (dotted line). (B) Potential step from −0.292 to −0.022 V, showing signals from heme b_L. (C) Potential step from −0.022 to 0.208 V, showing signals from heme b_H and partially signals from quinone. (D) Potential step from 0.208 to 0.708 V, showing signals from heme c_1 and the Rieske iron−sulfur protein. (E) Sum of spectra B−D. The dotted line in panel E represents the spectrum of the whole complex.

5C). This difference spectrum was calculated by subtracting a spectrum that includes signals from cytochrome c_1 and the Rieske protein (0.208−0.708 V, Figure 2D) from a spectrum that includes the signals from heme b_H, cytochrome c_1, the Rieske protein, and the quinones (potential step from −0.022 to 0.708 V, not shown). In this double-difference spectrum, contributions from all bound quinones and in addition from heme b_H are involved. The data confirm that the quinones dominate the spectra (more details about the vibrational modes of the quinones are given later in the text).

The b_H spectrum is dominated by several signals in the amide I region, and smaller modes can be found in the amide II range. Also here, similarities to the spectrum from *Rb. capsulatus* are obvious, and only minor shifts in the band position occur, especially in the amide I range. This region exhibits a dominant signal at 1656 cm^{-1}, most probably due to α-helical structure elements of the cytochrome *b* subunit, as found previously for the heme b_L. Most of the other signals can be tentatively assigned to contributions of the porphyrin ring. Candidates for vibrations of protonated heme propionates are the modes at 1692 and 1680 cm^{-1}, while contributions of the deprotonated form are likely at 1560 and 1540 cm^{-1}. The signal at 1620 cm^{-1} is a candidate for a vibration of the vinyl substituents, and the ν_{37} vibration from the porphyrin ring could contribute to the small signals at 1604 and 1582 cm^{-1}. The ν_{38} vibration, together with the amide II vibration and COO^- modes from deprotonated heme propionates and amino acid side chains, contributes to the signal at 1550 cm^{-1}. The *CmH* deformation vibration (ν_{42}) was previously identified at 1236 cm^{-1} and can assigned to the negative signal at 1240 cm^{-1} (*14*).

Several signals can be identified at positions typical for contributions of amino acid side chains. Signals at 1740 and 1710 cm^{-1} can be assigned to the C═O group of protonated aspartic and glutamic acid residues, and describe the reorganization of the acidic group upon electron transfer and coupled protonation reactions. In this case, the corresponding $\nu(COO^-)^{as}$ mode is expected to be between 1574 and 1560 cm^{-1} on the basis of studies on isolated Asp and Glu (*31*). In the respective spectral range, difference signals can be found at 1560 and 1540 cm^{-1}. The symmetric COO^- mode can be expected at approximately 1400 cm^{-1}, where small signals are present. However, a conclusive assignment is not possible without supporting data from mutants.

Previous studies on isolated amino acids show typical signals of Arg, Asn, and Gln at approximately 1670−1680 cm^{-1} and around 1620−1630 cm^{-1} (*31*). For Gln, additional modes are found at 1610 and 1590 cm^{-1}. In the presented difference spectrum (Figure 2C), relevant signals can be seen at 1680 and 1670 cm^{-1}, as well at 1630 and 1620 cm^{-1}. Baymann et al. (*14*) assign contributions from an Arg at 1676 and 1642 cm^{-1} in the heme b_H spectrum; in our spectrum, we found signals at 1670 and 1630 cm^{-1}. In the cytochrome *b* amino acid sequence, several highly conserved candidates that may be discussed here are present: Arg85 (Arg70 with the equivalent yeast numbering), Arg94 (Arg79), Arg114 (not conserved in yeast, but Lys99 is making an identical salt bridge with the heme propionate), Asn99 (Asn83), or Asn279 (Asn256) (*8*, *43*). These amino acid contributions will be conclusively assigned in mutant proteins.

Contributions of Heme c_1 and the Rieske ISP. Figure 2D shows the oxidized-minus-reduced spectrum for a potential step from 0.208 to 0.708 V, where signals from redox-dependent changes of heme c_1 and the Rieske ISP appear. We note that the midpoint potentials of both cofactors are

close (see above). Therefore, a strict separation was not possible, and a small overlap of the contributions has to be considered. The spectral features derived from heme c_1 and the ISP are significantly smaller than the overall spectrum of the bc_1 complex. Nevertheless, several clear signals can be found, mainly in the amide I region. As mentioned before, the FeS cluster of the Rieske protein itself will contribute at wavenumbers below 1000 cm^{-1}. However, signals from conformational changes in the polypeptide backbone that surrounds the cluster and is involved in the electron transfer reaction can be perceived in the measured range. For cytochrome c_1, modes of the heme and the environment of the cofactor are expected. As is known from mitochondrial bc_1 structures, cytochrome c_1 is a predominantly α-helical protein, whereas the catalytic domain of the Rieske protein comprises three layers of antiparallel β-sheets to yield a relatively compact and rigid extrinsic domain, which is connected to a transmembrane anchor helix by a flexible linker. Signals originating from the reorganization of this structure elements (amide I) coupled to the electron transfer can be expected in the IR spectrum.

In the amide I region, larger positive modes can be seen at 1698, 1680, 1658, and 1636 cm^{-1}, with a smaller signal present at 1646 cm^{-1}, and negative signals can be found at 1672 and 1630 cm^{-1}. The signals at 1698 and 1636 cm^{-1} could indicate reorganizations in the β-sheet structure of the Rieske ISP, whereas the signal at 1658 cm^{-1} might represent changes in α-helical structure elements of heme c_1 or in the membrane anchor of the Rieske ISP. Conformational modifications in the loop structure of the flexible linker region of the Rieske protein during the movement of the extrinsic domain as described in the literature (*4*, *32*) may be expected around 1680 cm^{-1}. In contrast, contributions of structurally unordered parts or helical turns in this loop will contribute at 1646 cm^{-1}.

Besides the signals of the secondary structure elements, contributions of heme *c* are expected. The protonated heme propionates could contribute to the positive mode at 1680 cm^{-1}, and the corresponding signals of the deprotonated form are likely between 1560 and 1524 cm^{-1}. In contrast to the *b*-type hemes, no vinyl substituents are present in *c*-type hemes, due to thioether bonds to cysteine side chains of the protein.

The bands at 1598, 1548, and 1566 cm^{-1}, with a shoulder at 1576 cm^{-1}, may result from amide II vibrations. This assumption is supported by a decrease in the magnitude of the 1548 cm^{-1} signal and a shift of the signal at 1566 cm^{-1} after H−D exchange (data not shown). Additional signals are expected from the porphyrin ring of heme c_1; the mode at 1598 cm^{-1} and the shoulder at 1576 cm^{-1} show no absorption changes after H−D exchange and are possible candidates for the *CaCm* vibration of the heme porphyrin ring. The mode at 1548 cm^{-1} could partially result from the *CbCb* vibration, whereas the *CaN* mode of the porphyrin ring might contribute to the small signals at 1338 and 1330 cm^{-1}.

To assign the signals in Figure 2D to either cytochrome c_1 or the Rieske ISP, we investigated water-soluble fragments. Figure 3B shows the electrochemically induced oxidized-minus-reduced FTIR difference spectrum of the isolated water-soluble cytochrome c_1 fragment (note that the spectrum was enlarged 5-fold). The amide I region exhibits

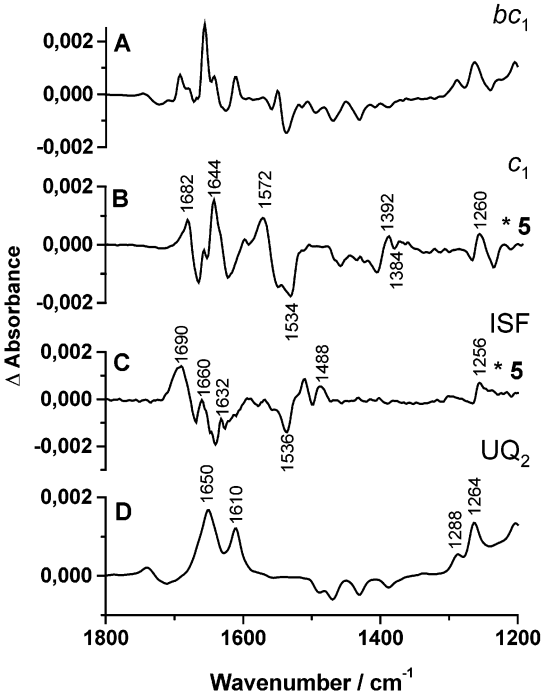

FIGURE 3: Oxidized-minus-reduced FTIR spectra of isolated components of the bc_1 complex from *P. denitrificans* for a potential step from −0.292 to 0.708 V: whole complex (A), cytochrome c_1 fragment (B), Rieske iron−sulfur protein fragment (C), and free ubiquinone UQ_2 in solution (D). The spectra are normalized to the same concentration. Spectra in panels B and C are magnified 5-fold.

two positive bands at 1682 and 1644 cm^{-1} and a smaller mode at 1658 cm^{-1} that include the C═O stretch vibrations of the polypeptide backbone. The mode at 1658 cm^{-1} also points to α-helical structure elements involved here. However, most of the dominant bands may be attributed to the *c* heme itself. The signal at 1682 cm^{-1} is present in all spectra where reactions of cytochrome c_1 are involved, and is overlapped by a strong signal at 1680 cm^{-1} in the spectra of the whole complex (Figures 1A and 2D). We tentatively assign these bands to the COOH modes of one of the heme propionates. The $\nu(COO^-)^{as}$ vibration of the deprotonated heme propionates may contribute to the signals at 1534 and 1552 cm^{-1}, whereas the $\nu(COO^-)^{s}$ vibration could be attributed to the negative signal at 1384 cm^{-1}. The large modes at 1644 and 1572 cm^{-1} are candidates for the *CaCm* (ν_{37}) and *CbCb* (ν_{38}) vibrations of the heme porphyrin ring, respectively. Overlaps from the amide II band and the COO^- vibration of deprotonated acidic amino acid side chains are possible. A positive signal at 1392 cm^{-1} is in the range where the *CaN* (ν_{41}) vibration is expected. Another noteworthy band can be identified at 1260 cm^{-1}, and is tentatively assigned to the *CmH* (ν_{42}) mode of the *c* heme. In previous studies of water-soluble *c*-type cytochromes (*33*, *34*), this signal was attributed to a tyrosine C−O stretch vibration. However, in the spectrum shown here, we could not identify significant modes in the spectral region characteristic for tyrosine, such as the prominent mode at 1518 cm^{-1}.

Figure 3C shows the difference spectrum of the water-soluble fragment of the Rieske protein (ISF). The fragment comprises only the redox-active domain, lacking the N-terminal membrane anchor and the flexible linker. The band structure is very similar to that found for the isolated Rieske protein fragment from beef heart mitochondria (*35*) and the

calculated difference spectrum of the Rieske protein from *Rb. capsulatus* (*14*). The peak positions of these spectra only differ by a few wavenumbers, and the peak intensities vary slightly, an effect probably based on subtle differences in each protein. In Figure 3C, a prominent band is present at 1690 cm^{-1}. This is a characteristic signal for Rieske proteins that was previously assigned to the amide I mode of the predominantly β-sheet secondary structure (*35*). Other signals partially involved in the C═O vibration of the polypeptide backbone can be found at 1660 cm^{-1} (α-helical and unordered regions) and 1632 cm^{-1} (β-sheet structure). This assignment is supported by a band shift of 5 cm^{-1} for the first mode and 12 cm^{-1} for the second mode after H−D exchange (data not shown), excluding a contribution from Asn, Gln, or Arg, since a major shift of the C═O vibrational mode and the CN_3H_5 mode, respectively, would be expected (*31*, *45*).

A strong negative signal identified at 1536 cm^{-1} and positive signals present at 1568, 1510, and 1488 cm^{-1} can be tentatively assigned to the coupled CN/NH modes of the amide II vibration. Contributions from individual amino acid side chains are possible, but conclusive assignments are difficult because of several overlapping bands from the amide II mode. The [2Fe-2S] cluster is coordinated by cysteine and histidine residues. The histidine ring vibration is expected at 1596 cm^{-1}, but the signal intensity is too low for an identification in the spectrum. A positive signal is present at 1256 cm^{-1}, which may tentatively be assigned to a tyrosine mode.

Contributions of the Quinones. The overall spectrum of the *P. denitrificans* bc_1 complex (Figure 1A) is dominated by modes of the bound quinone. This can be clearly demonstrated by comparison with spectra of free quinone in solution. The spectrum in Figure 3D shows the oxidized-minus-reduced FTIR difference spectrum of the ubiquinone UQ_2 in aqueous solution, as previously obtained (*36*) for a potential step from −0.292 to 0.708 V. The IR spectroscopic properties of the free UQ_2 in solution are very similar to those of the endogenous UQ_{10} from *P. denitrificans* (*37*). The positive signals at 1650, 1610, 1288, 1264, and 1204 cm^{-1} correlate with the neutral quinone, while the negative signals at 1490, 1470, 1432, and 1388 cm^{-1} represent the reduced and protonated quinol form. The mode at 1650 cm^{-1} was previously assigned to the C═O vibration of the quinone, whereas the mode at 1610 cm^{-1} was attributed to the C═C vibration. The C−O modes of the methoxy groups contribute to the signals at 1288 and 1264 cm^{-1}. Reorganizations of the quinone ring likely lead to the negative signals present in the spectrum.

All difference signals of the quinone in solution can clearly be identified in the overall spectrum of the bc_1 complex shown in Figure 3A. The C═O vibrational mode of the bound quinone splits into two bands at 1656 and 1642 cm^{-1}, depending on different hydrogen bonding. The C═C vibration of the quinone ring, a mode that is rather unsensitive to the environment, can be tentatively assigned to the band at 1610 cm^{-1} (*14*). These signals become more distinct due to formation of hydrogen bonds as well as changes in the orientation and configuration of the quinone upon binding. Signals from 1500 to 1430 cm^{-1} may be attributed to the ring modes of the fully reduced and protonated forms of ubiquinol (*14*, *36*). At 1288 and 1262 cm^{-1}, the C−OCH_3 vibrations of the neutral quinone methoxy groups contribute to the spectrum.

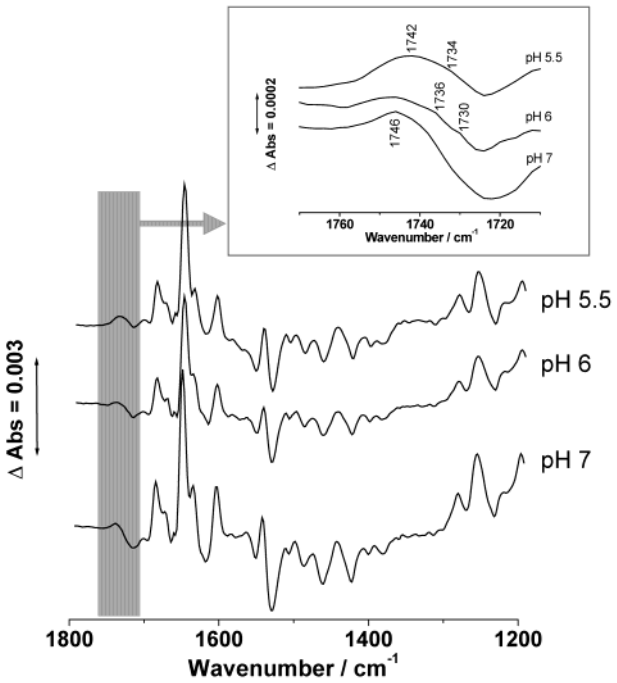

FIGURE 4: Oxidized-minus-reduced FTIR difference spectra of the bc_1 complex from *P. denitrificans* in phosphate buffer (pH 6 and 7) and cacodylate buffer (pH 5.5) for the potential step from −0.292 to 0.708 V. The inset shows the enlarged view of the spectra from 1770 to 1710 cm^{-1}. Spectra are normalized to the same concentration according to the α-band in the visible spectral range.

Protonation of Acidic Groups upon Quinone Binding. Measurements under different pH conditions provide additional information about protonatable groups and redox relevant amino acid side chains of the enzyme. The spectra recorded at pH 5.5, 6, and 7 are shown in Figure 4. Spectra recorded at pH 8 are not given here, because the complex was not stable at the applied potentials and the loss of redox reactivity of heme *b* was observed in the visible region. Figure 4 shows the normalized oxidized-minus-reduced FTIR difference spectra determined for a potential step from −0.292 to 0.708 V. The three spectra are similar, but differences in the signal intensity and peak position can be seen. In detail, in the spectra recorded at pH 5.5 and 6, different small signals in the range from 1730 to 1750 cm^{-1} can be identified, indicating that several protonated groups are involved here (see the enlarged inset). In the spectrum obtained for the sample at pH 7, a band at 1746 cm^{-1} can be identified. At pH 6, this band becomes broader and additional shoulders at 1736 and 1730 cm^{-1} appear. Concomitant with the decrease to pH 5.5, the maximum of the broad band shifts to 1742 cm^{-1}, the shoulder at 1736 cm^{-1} can be only weakly observed, and the shoulder at 1730 cm^{-1} disappears. The bands previously assigned to the bound quinone are also affected. In detail, a decrease in the magnitudes of the signals at 1610, 1468, 1430, 1288, and 1262 cm^{-1} is observable. We assume a relationship between the protonation signals shown in Figure 4 and the quinone content of the sample, which obviously differs depending on sample preparation. To probe this suggestion, samples with different quinone contents have been compared (Figure 5A). The solid line represents the lowest quinone content,

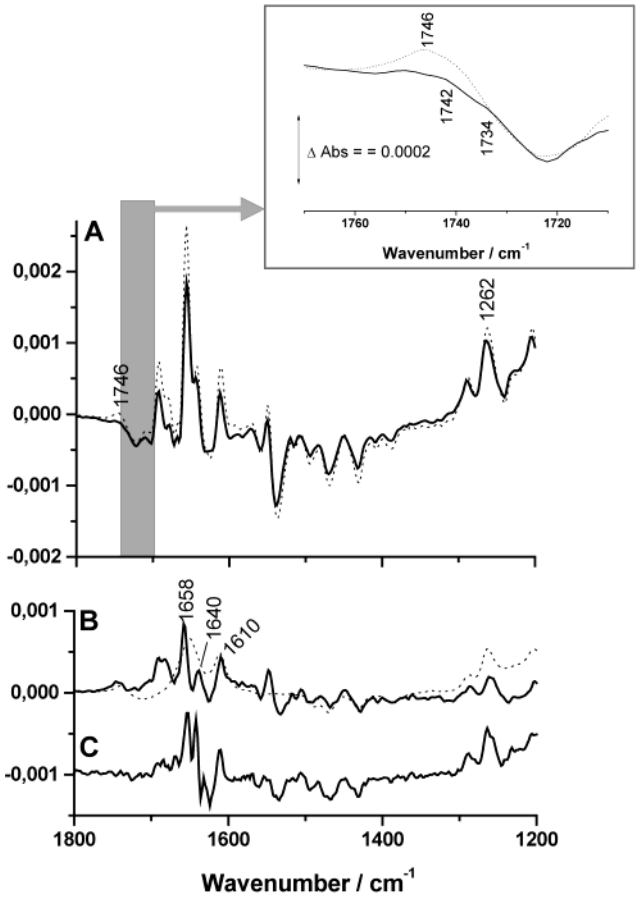

FIGURE 5: (A) Comparison of oxidized-minus-reduced FTIR difference spectra of the bc_1 complex from *P. denitrificans* in phosphate buffer (pH 7) for the potential step from −0.292 to 0.708 V with different quinone content. The variation is based on the handling of the sample during the last concentration step (see Materials and Methods). The thick line represents a sample with a low quinone content and the dotted line a spectrum with a higher quinone content. The inset shows the enlarged view of the spectra from 1770 to 1710 cm^{-1}. The spectra are normalized to the same protein concentration as observed in the visible spectral range. (B) Double-difference spectrum of the spectra given in panel A (solid line) in comparison to the spectrum of free UQ_2 (dotted line), signals originating likely from the quinone bound at the Q_o site. In comparison, the spectrum for all bound quinones (C) is given, calculated on the basis of selected potential steps (for details, see the text).

and the dotted line represents the highest content found in our experiments at pH 7. The quinone content in the different samples ranged from 2.6 to 3.3 molecules per monomer, based on the signal intensity at 1262 cm^{-1} ($\epsilon = 0.4$ mM^{-1} cm^{-1}).

The double-difference spectrum (Figure 5B) demonstrates the vibrations of quinones most likely originating from the Q_o site. This assumption is based on the double-occupancy model of Ding (*12*), which postulates a weakly bound quinone at Q_o that can be removed easily. The position of the C═O modes at 1658 cm^{-1} and probably at 1640 cm^{-1} and the signal shape clearly exclude any unspecifically bound quinone. The quinone can be easily removed by buffer exchange procedures. For a comparison, Figure 5C shows signals of all bound quinones. This spectrum also includes the small signals of heme b_H (see Figure 2C) and was determined as described previously. On the basis of the quinone midpoint potentials, at the Q_o or Q_i site, the different quinones are indistinguishable for the given pH and the chosen potential step.

The inset in Figure 5 shows an enlarged view of the region from 1770 to 1710 cm^{-1}. The signal at 1746 cm^{-1}, only present in the high-quinone content bc_1 preparation, disappears with a decrease in quinone content, whereas additional signals at 1742 and 1734 cm^{-1} appear. These effects have been observed similarly in the spectra in Figure 4. In the spectrum obtained at pH 7 with a higher quinone content, the mode at 1746 cm^{-1} is present, and bands at 1742 and 1734 cm^{-1} could be identified in the pH 5.5 spectrum, which contains a smaller amount of quinone. From our results, we can conclude there is a combination of two effects. (I) The quinone content can be decreased by concentration and redilution of the protein sample, and (II) the quinone binding affinity is also affected by pH conditions. Acidic pH values decrease the quinone content.

CONCLUSIONS

This study is the first FTIR spectroscopic characterization of the bc_1 complex from *P. denitrificans*. Electrochemically induced difference spectra of the complex clearly show contributions of all cofactors (Figure 1A), and are dominated by modes from bound quinones. The tentative assignments made in this report are summarized in Table 1. The quinone content of the sample strongly depends on the sample preparation and buffer exchange procedures before the FTIR measurements are carried out (Figure 5). We determined the quinone concentration on the basis of the absorption properties of the methoxy group at 1262 cm^{-1}. The signals of this group are only weakly affected by binding of quinone to the protein. We estimated a ratio of 2.6−3.3 molecules per monomer of the bc_1 complex, depending on the preparation. This corresponds to the high quinone content of the *P. denitrificans* complex found by Yang et al. (*38*). In mitochondrial complexes, Bartoschek et al. (*39*) reported three quinones bound to the complex, whereas crystal structures reveal only one quinone in the Q_i site (*4*, *5*, *40*, *41*). For the Q_o occupancy, two different models are discussed, named, the single-occupancy model (*9*) and the double-occupancy model (*12*). Our results more likely support the double-occupancy model with two quinones bound in the Q_o site.

In addition, we found a pH dependency of the quinone content, linked to the amplitude of protonation signals in the spectral region around 1740 cm^{-1}. The signal at 1746 cm^{-1} (Figure 1A) correlates with high quinone concentrations. As a likely possibility, one or more protonated Glu or Asp side chains are involved in the redox reaction. This group(s) is deprotonated upon quinone release since the magnitude of the signal decreases with a lower quinone content in the sample (Figure 5). Bands at 1742 and 1734 cm^{-1} are found in spectra with lower quinone content. Possible candidates in the cytochrome *b* subunit are Glu295, Asp252, Asp86, Asp278, and E415 (*P. denitrificans* numbering; *43*), which are all conserved in most of the bacterial and mitochondrial bc_1 complexes (*8*, *43*). Glu295 corresponds to Glu272 in mitochondrial complexes and is probably involved in quinone liganding at the Q_o site. Asp252 is equivalent to Asp229 in mitochondrial complexes and is located at the Q_i site. Further assignments of individual side

chains involved in the cytochrome bc_1 reaction cycle will be performed in combination with site-directed mutagenesis in the future.

ACKNOWLEDGMENT

We are grateful to Anna Eichhorn for providing the soluble cytochrome c_1 fragment and Klaus Zwicker for performing the EPR spectroscopy on the soluble Rieske fragment.

REFERENCES

1. Berry, A. B., Guergova-Kuras, M., Huang, L., and Crofts, A. R. (2000) *Annu. Rev. Biochem. 69*, 1005−1075.
2. Hunte, C., Koepke, J., Lange, C., Rossmanith, T., and Michel, H. (2000) *Structure 8*, 669−684.
3. Iwata, S., Lee, J. W., Okada, K., Lee, J. K., Iwata, M., Rasmussen, B., Link, T. A., Ramaswamy, S., and Jap, B. K. (1998) *Science 281*, 64−71.
4. Zhang, Z., Huang, L., Shulmeister, V. M., Chi, Y., Kim, K. K., Hung, L. W., Crofts, A. R., Berry, E. A., and Kim, S. H. (1998) *Nature 392*, 677−684.
5. Xia, D., Yu, C. A., Kim, H., Xia, J. Z., Kachurin, A. M., Zhang, L., Yu, L., and Deisenhofer, J. (1997) *Science 277*, 60−66.
6. Mitchell, P. (1976) *J. Theor. Biol. 62*, 327−367.
7. Trumpower, B. L. (1990) *J. Bioenerg. Biomembr. 23*, 241−255.
8. Brandt, U., and Trumpower, B. (1994) *Crit. Rev. Biochem. Mol. Biol. 29*, 165−197.
9. Crofts, A. R., and Wang, Z. (1989) *Photosynth. Res. 22*, 69−87.
10. Link, T. A. (1997) *FEBS Lett. 412*, 257−264.
11. Brandt, U. (1996) *FEBS Lett. 387*, 1−6.
12. Ding, H., Moser, C. C., Robertson, D. E., Tokito, M. K., Daldal, F., and Dutton, P. L. (1995) *Biochemistry 34*, 15979−15996.
13. Sharp, R. E., Gibney, B. R., Palmitessa, A., White, J. L., Dixon, J. A., Moser, C. C., Daldal, F., and Dutton, P. L. (1999) *Biochemistry 38*, 14973−14980.
14. Baymann, F., Robertson, D. E., Dutton, P. L., and Mäntele, W. (1999) *Biochemistry 38*, 13188−13199.
15. Hellwig, P., Behr, J., Ostermeier, C., Richter, O. M., Pfitzner, U., Odenwald, A., Ludwig, B., Michel, H., and Mäntele, W. (1998) *Biochemistry 37*, 7390−7399.
16. Hellwig, P., Scheide, D., Bungert, S., Mäntele, W., and Friedrich, T. (2000) *Biochemistry 39*, 10884−10891.
17. Pfitzner, U., Odenwald, A., Ostermann, T., Weingard, L., Ludwig, B., and Richter, O. M. (1998) *J. Bioenerg. Biomembr. 30*, 89−97.
18. Korn, M. (1994) Diploma Thesis, Johann Wolfgang Goethe-Universität, Frankfurt am Main, Germany.
19. Schröter, T., Hatzfeld, O. M., Gemeinhardt, S., Korn, M., Friedrich, T., Ludwig, B., and Link, T. A. (1998) *Eur. J. Biochem. 255*, 100−106.
20. Ludwig, B., Suda, K., and Cerletti, N. (1983) *Eur. J. Biochem. 137*, 597−602.
21. Link, T. A., Saynovits, M., Assmann, C., Iwata, S., Ohnishi, T., and von Jagow, G. (1996) *Eur. J. Biochem. 237*, 71−75.
22. de Vries, S., Cherepanov, A., Berg, A., and Canters, G. W. (1998) *Inorg. Chim. Acta 275−276*, 493−499.
23. Eichhorn, A. (2003) Ph.D. Thesis, Johann Wolfgang Goethe-Universität, Frankfurt am Main, Germany.
24. Moss, D., Nabedryk, E., Breton, J., and Mäntele, W. (1990) *Eur. J. Biochem. 187*, 565−572.
25. Mäntele, W. (1993) *Trends Biochem. Sci. 18*, 197−202.
26. Mäntele, W. (1996) in *Biophysical Techniques in Photosynthesis* (Hoff, A. J., and Amesz, J., Eds.) Chapter 9, pp 137−160, Kluwer, Dordrecht, The Netherlands.
27. Trumpower, B. L. (1990) *Microbiol. Rev. 54*, 101−129.
28. Berthomieu, C., Boussac, A., Mäntele, W., Breton, J., and Nabedryk, E. (1992) *Biochemistry 31*, 11460−11471.
29. Behr, J., Hellwig, P., Mäntele, W., and Michel, H. (1998) *Biochemistry 37*, 7400−7406.
30. Hellwig, P., Grzybek, S., Behr, J., Ludwig, B., Michel, H., and Mäntele, W. (1999) *Biochemistry 38*, 1685−1694.
31. Venyaminov, S. Y., and Kalnin, N. N. (1990) *Biopolymers 30*, 1243−1257.
32. Crofts, A. R., Guergova-Kuras, M., Huang, L., Kuras, R., Zhang, Z., and Berry, E. A. (1999) *Biochemistry 38*, 15791−15806.
33. Schlereth, D., and Mäntele, W. (1993) *Biochemistry 32*, 1118−11126.
34. Baymann, F. (1991) Diploma Thesis, Albert-Ludwigs-University, Freiburg, Germany.
35. Baymann, F. (1995) Ph.D. Thesis, Albert-Ludwigs-University, Freiburg, Germany.
36. Hellwig, P., Mogi, T., Tomson, F. L., Gennis, R. B., Iwata, J., Miyoshi, H., and Mäntele, W. (1999) *Biochemistry 38*, 14683−14689.
37. Bauscher, M., and Mäntele, W. (1992) *J. Phys. Chem. 96*, 11101−11108.
38. Yang, X., and Trumpower, B. L. (1986) *J. Biol. Chem. 261*, 12282−12289.
39. Bartoschek, S., Johansson, M., Geierstanger, B. H., Okun, J. G., Lancaster, C. R., Humpfer, E., Yu, L., Yu, C. A., Griesinger, C., and Brandt, U. (2001) *J. Biol. Chem. 276*, 35231−35234.
40. Kim, H., Xia, D., Yu, C. A., Xia, J. Z., Kachurin, A. M., Zhang, L., Yu, L., and Deisenhofer, J. (1998) *Proc. Natl. Acad. Sci. U.S.A. 95*, 8026−8033.
41. Hunte, C. (2001) *FEBS Lett. 25152*, 1−7.
42. Lange, C., and Hunte, C. (2002) *Proc. Natl. Acad. Sci. U.S.A. 99*, 2800−2805.
43. Kurowski, B., and Ludwig, B. (1987) *J. Biol. Chem. 262*, 13805−13811.
44. Yang, X., and Trumpower, B. (1988) *J. Biol. Chem. 263*, 11962−11970.
45. Goormaghtigh, E., Cabiaux, V., and Ruysschaert, J. M. (1994) *Subcell. Biochem. 23*, 405−450.
46. Salerno, C. S., Xu, Y., Osgood, M. P., Kim, C. H., and King, T. E. (1989) *J. Biol. Chem. 264*, 15398−15403.

BI035103J